Applied Surface Science 528 (2020) 146917

Contents lists available at ScienceDirect

Applied Surface Science

journal homepage: www.elsevier.com/locate/apsusc

Full Length Article

Reversible graphitization of SiC: A route towards high-quality graphene on a minimally step bunched substrate

Piotr Ciochoń[a,*], Mateusz Marzec[b], Natalia Olszowska[c], Jacek Kołodziej[a,c]

[a] Institute of Physics, Faculty of Physics, Astronomy and Applied Computer Science, Jagiellonian University, ul. prof. Stanisława Łojasiewicza 11, 30-348, Cracow, Poland
[b] Academic Centre for Materials and Nanotechnology (ACMiN), AGH University of Science and Technology, Av. Mickiewicza 30, 30-059 Krakow, Poland
[c] National Synchrotron Radiation Centre SOLARIS, Jagiellonian University, Czerwone Maki 98, 30-392 Kraków, Poland

ARTICLE INFO

Keywords:
Graphene
Silicon carbide
Synthesis
Surface

ABSTRACT

We show that the thermal decomposition of SiC (0001) surface is reversible, if carried out in near-equilibrium conditions, with an external Si atomic beam applied to the substrate. Taking advantage of this observation we design a novel process, allowing for the growth of uniform, few-layers, ABC-stacked graphene. This process is composed of two phases; the first is a graphene film growth and the second is its reduction to the desired thickness. We find that, when using this scheme instead of the conventional ones the heavy step bunching on the substrate is avoided, and the step heights remain below 2.75 nm.

Since the step bunching is one of the most important factors prohibiting the use of epitaxial graphene on SiC in certain application areas, such as analog electronics or sensing, our method has the potential to be applied in future wafer-scale graphene technologies and processes. Moreover, the results obtained in this work exemplify general near-equilibrium phenomena and therefore they may be also relevant for growth methods of other 2D materials.

1. Introduction

Thermal graphitization of the Si-terminated SiC (0001) surface, is one of the few available methods, allowing for wafer-scale production of homogeneous, epitaxial graphene films, possibly useful for the development of graphene electronic technology [1,2,3]. Although the SiC graphitization process, occurring due to preferential Si sublimation from the SiC wafer's surface at high-temperatures, has been known for long time [4], it was the introduction of atmospheric pressure [5] and confinement controlled SiC graphitization [6] methods, which enabled a production of high-quality material, able to compete with the CVD graphene [7,8,9]. In recent years, a few new variants of the thermal SiC graphitization have been investigated, including graphitization of the C-terminated surface (which is less controllable, but results in the material characterized by higher electron mobility [10,11]), graphitization of SiC vicinal surfaces [12], or thermal growth of graphene nanoribbons on patterned SiC [13].

Despite wide ongoing research, many phenomena, occurring during graphene growth via surface thermal decomposition of SiC, remain only partially understood and controlled. In particular, the formation of macro-steps, with the height of several tens of nanometers on the graphene covered SiC surface, via the step-bunching mechanism, and bilayer-patches on graphene film near the step edges, are especially problematic. These issues are considered the main obstacles on the road to the future graphene/SiC-based electronics [14]. Several countermeasures to these unwelcomed phenomena have been studied, including tuning the heating rate of the SiC wafer [15], or using polymer masks, serving as a source material for buffer layer formation [16].

Here, we investigate an alternative method to control the process of SiC thermal graphitization in UHV using Si atomic beam from an external source to slow down the Si loss from the surface. We find, that the process of graphene film formation is reversible in such circumstances. Si atomic beam allows to increase the process temperature and to grow uniform few-layers graphene. This graphene is crystallographically highly ordered and characterized by the ABC-type stacking of the layers. We also show that, in contrast to previous studies that did not use the Si beam, low heating rates, which are desirable for obtaining good crystallographic order, do not lead to the step-bunching and the graphene/SiC surface remains free of macro-steps. This is attributed to the preferential adsorption of Si atoms at the step edges.

2. Experimental details

Prior to the graphene growth, epi-ready samples of 4H-SiC exposing

* Corresponding author.
E-mail address: piotr.ciochon@doctoral.uj.edu.pl (P. Ciochoń).

https://doi.org/10.1016/j.apsusc.2020.146917
Received 24 January 2020; Received in revised form 5 May 2020; Accepted 4 June 2020
Available online 10 June 2020

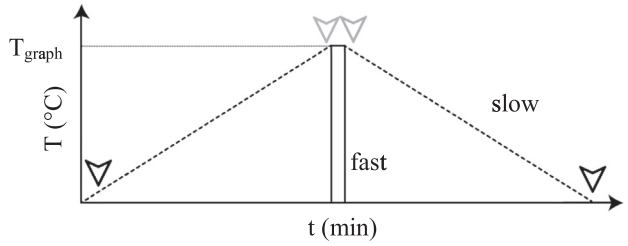

Fig. 1. Scheme of the two variants of graphitization used in the experiments, utilizing either: fast (solid line) or slow (dashed line) heating/cooling rate and annealing at the graphitization temperature T_{graph} (time is not to scale); arrows represent times when the flux of Si atoms was switched on and off (black for the slow and grey for fast heating/cooling.

(0001) surface were rinsed with IPA, introduced into the UHV chamber, degassed, and annealed in the Si beam with the density of 6×10^{12} cm^{-2} s^{-1}, at the temperature equal to 900 °C, to form a clean, 3 × 3-reconstructed surface. The growth was carried out in temperatures of 1450–1900 °C while the SiC surface was exposed to the Si beam of 1.8–2.5 × 10^{14} cm^{-2} s^{-1}. The sample heater used for the growth process was of electron beam type, with the electrons bombarding directly the backside of the sample. This technique allowed for precise and quickly responding control of the process temperature. The wafer temperature was measured using an infrared pyrometer. Heating and cooling rates of the SiC substrate were controlled and, in most experiments, they were either slow (0.35 °C/min if not stated differently) or fast (~100 °C/s). Schemes of the two processes are shown in Fig. 1

In case of slow heating/cooling, the flux of Si atoms is applied to the surface already at the temperature of ~900 °C (i.e. the temperature of the formation of the 3 × 3 reconstructed surface), well below graphitization temperatures, and it is not switched off until the sample cools down to the same temperature. The complete process takes between 20 and 40 min.

Synthesized graphene was characterized with use of X-ray photoelectron spectroscopy (XPS), angle-resolved photoelectron spectroscopy (ARPES), low energy electron diffraction (LEED) and the intermittent-contact (tapping) atomic force microscopy (AFM). The synthesis as well as spectroscopic and diffraction measurements were performed in a single UHV system, with the base pressure < 1 × 10^{-10} mbar. VG-Scienta R4000 hemispherical analyzer with VUV5k UV lamp or a PREVAC RS 40B1 X-ray source using Mg anode were used for the photoelectron experiments and OCI MCP LPS300-D diffractometer was used for LEED studies. AFM measurements were performed in air, using NanoSurf EasyScan microscope, with ACL-A tips. ARPES and ARXPS measurements were partially performed at ARPES beamline of the National Synchrotron Radiation Centre SOLARIS, after transferring the samples in air. XPS measurements were partially performed at the Academic Centre for Materials and Nanotechnology, using PHI 5000 VersaProbe II spectrometer, after transferring the samples in air. Si atomic beam was obtained with a MBE Komponenten SUSI Si sublimation source.

3. Results and discussion

As the first step we investigate the reversibility of graphene formation on SiC (0001) surface. We prepare a partly-graphitized sample, by annealing it using the fast scheme, in the temperature of 1352 °C and with the Si flux of 1.8 × 10^{14} cm^{-2} s^{-1}, for 5 min. The C1s region of the XPS spectrum of the sample, is shown in Fig. 2a. It consists of 4 components labeled: G (E_B = 284.8 eV), related to graphene, S1 (E_B = 285.2 eV) and S2 (E_B = 285.8), related to the buffer layer and SiC (E_B = 283.9 eV), related to bulk substrate. This spectrum is in agreement with literature data [17]. The share of graphene-associated component is equal to ~25%, which corresponds to ~ 0.5ML coverage.

This partly-graphitized sample is further annealed (using the fast scheme), in a temperature T = 1347 °C, i.e. lowered by 5 °C, and in the same flux of Si atoms for 55 min (total annealing time equal to 60 min). The XPS spectrum of the sample is shown Fig. 2b. While previously described components (G, S1, S2, SiC) are still present, we observe an emergence of an additional, pronounced component (SiC′). The new component has a binding energy of E_B = 282.9 eV, which is shifted by around 1 eV to lower binding energies, relative to the bulk SiC component. This is accompanied by the relative decrease in the intensity of the G, SiC, S1 and S2 signals. The same sample is annealed again for 150 min (using the fast scheme), in an unchanged temperature (T = 1347 °C) and Si flux. The XPS spectrum for the sample after the two annealing steps (total annealing time equal to 210 min) is shown in Fig. 2c. As seen SiC, G, S1 and S2 are now replaced by a single component (labeled SiC′), i.e. the bulk component is shifted due to band bending and the surface components are not resolved. We have previously observed similar spectra for the 3 × 3-reconstructed SiC (0001) surfaces, [13], therefore we attribute SiC′ component to the ungraphitized, restored surface of SiC. The absence of graphene is confirmed by ARPES measurements for the same sample, shown in Fig. 2d. The ARPES spectrum is measured around the K point in the reciprocal space of the (previously present) graphene lattice and shows no presence of the Dirac cone, characteristic for graphene.

LEED diffraction pattern, characteristic for the 6R3 surface reconstruction is observed after annealing the sample for 60 min at 1347 °C (Fig. 2e), which indicates the presence of both graphitized and ungraphitized areas on the sample. After further annealing for 150 min, it is transformed into a complex, previously unobserved pattern (Fig. 2f). For this surface XPS indicates prevailing chemical carbon bonds similar to that of SiC(3 × 3), band bending similar to that observed for SiC(3 × 3) and no contamination peaks. AFM images of the sample, show that the surface is characterized by a regular terrace structure (Fig. 2g). The terraces have the width of around 1 μm and they are separated by steps with an average height of 2–3 nm. Detailed imaging reveals, that the terraces are covered with meandering, elongated pits (Fig. 2h), with the depth of around 0.25 nm (Fig. 2i). This depth is equal to the height of a single SiC bilayer (0.25 nm).

As shown in our previous work [18] applying an external flux of 1.8 × 10^{14} cm^{-2} s^{-1} Si atoms to the SiC surface annealed at T = 1350 °C can fully inhibit its graphitization. Thus, in a specific temperature (or temperature range), the incoming flux of Si atoms is equal to the Si flux emitted by the surface being annealed and the system is in the state of a dynamic equilibrium (SiC ⇌ Si + G). This situation is similar to one present during the high-pressure/confinement graphitization, in which “the silicon atoms desorbing from the surface have a finite probability of being reflected back to the surface” [5].

In the present experiment, the initial graphitization of the sample is performed in the temperature slightly above the temperature of this dynamic equilibrium which shifts the reaction towards the products side (Si + G). The following prolonged annealing is performed at the temperature slightly below the equilibrium temperature, for the applied Si flux, which shifts the reaction towards the reactant side (SiC substrate). This is significantly different from the high-pressure/confinement graphitization process, for which the incoming Si flux cannot be higher then the Si flux emitted from it. Formation of silicon carbide “islands” on a graphitized sample, annealed at temperatures of 1000–1100 °C after Si deposition, has been previously observed by Xia et. al. [19], but has not been invesitgated thoroughly. Our results show that the graphitization process on SiC(0001) is fully reversible, i.e. all the C–C bonds on surface may disappear, upon annealing the graphitized surface in Si flux, in the properly tuned near-equlibrium reaction conditions.

Fig. 3 shows core-level spectra of the Si 2p region for the sample annealed in T = 1347 °C, in Si flux of 1.8 × 10^{14} cm^{-2} s^{-1} (graphitization reversal in the temperature slightly below the equilibrium

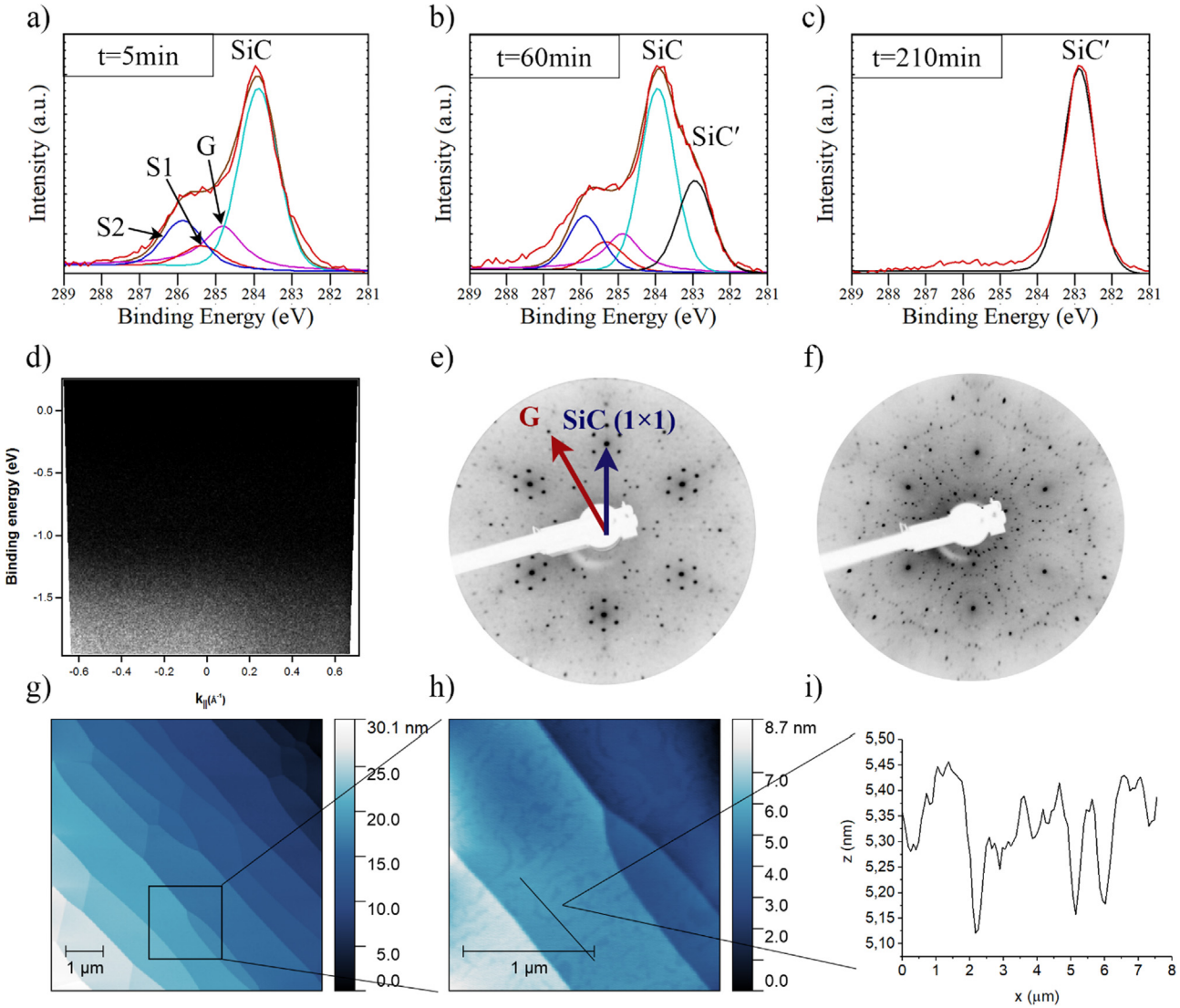

Fig. 2. XPS spectra of SiC sample annealed at: a) T = 1350 °C for 5 min, followed by the annealing of the same sample at 1347 °C: b) for 60 min; c) for additional 50 min (total annealing time equal to 110 min); components in the XPS spectra are assigned to: bulk SiC (SiC: light-blue), graphene (G: magenta), buffer layer (S1: red, S2: blue) and ungraphitized SiC (SiC′: black); d) ARPES spectrum around the K point of the reciprocal lattice of graphene, of the sample annealed at 1347 °C for the total time of 110 min, corresponding to the XPS spectrum shown in Fig. 2c; diffraction patterns of the sample annealed at 1347 °C for e) 60 min, corresponding to the XPS spectrum shown in Fig. 2b (incident electron energy E_{inc} = 189 eV), f) 210 min, corresponding to the XPS spectrum shown in Fig. 2c. (E_{inc} = 200 eV); diffraction spots and vectors related to the lattice of graphene and (1 × 1) SiC are marked in red and blue, respectively) AFM scan of the SiC sample annealed for the total time of 110 min (corresponding to the XPS spectrum shown in Fig. 2c and LEED pattern shown in Fig. 2f); h) detailed AFM scan of the area market by an inlet in Fig. 2g; i) line profile, taken along the line drawn in Fig. 2h.

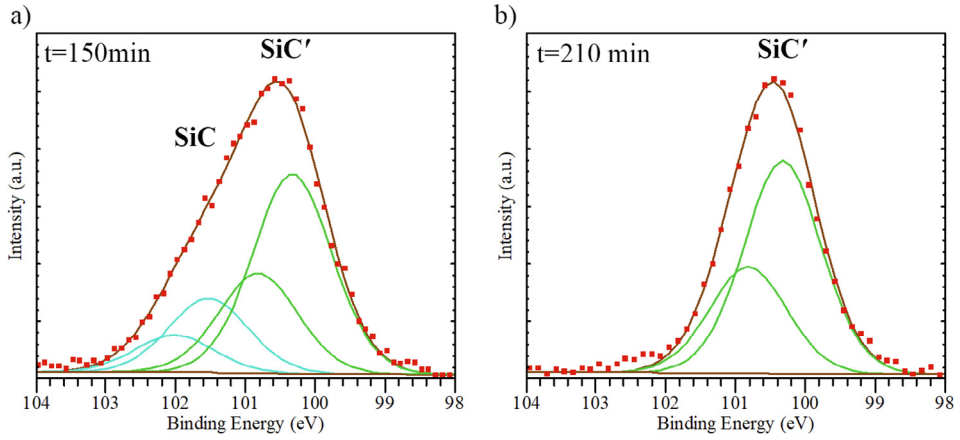

Fig. 3. XPS spectra, in the Si 2p region of the SiC sample annealed in the temperature slightly below the equilibrium temperature for: (a) 150 min and (b) 210 min.

temperature) for 150 min and 210 min.

Spectra in the Si 2p region can be fitted with a pair of 2p doublets (corresponding to the $2p_{1/2}$ and $2p_{3/2}$ energy levels, with the area ratio of 1:2), in the case of annealing time equal to 150 min, or ~~by~~ with a single doublet, in the case of annealing time equal to 210 min. The separation between the doublets is equal to around 1 eV, which is the same as the observed shift between the SiC and SiC′ components in the C1s region of the spectrum. Therefore they can be assigned to the SiC and SiC′ phases in accordance with the band bending effect recognized as a mechanism leading to the observed XPS peak shifts. XPS data indicates that there are no measurable number of Si-Si bonds on the samples with SiC′ phase.

In order to gain an understanding of the mechanism of SiC re-growth we have performed a soft-XPS (SXPS) measurements at the UARPES beamline of the National Synchrotron Radiation Centre SOLARIS on a sample, for which the graphene coverage was decreased from around 1.5ML to around 0.7ML through graphitization reversal. The SXPS spectra have been measured, for the photoelectron emission angles 0° and 65°, with respect to the surface normal, and for the photon energies (PhE) in the range 320–600 eV. It is important to note, that for these photon energies, the inelastic mean free path of the photoelectrons is around its minimum and corresponds to 1–2 atomic layers at 400 eV PhE and 2–3 atomic layers at 600 PhE [20]. It makes this method very surface sensitive, depending also on the tilt applied to the sample. In the Fig. 4 we show data for 600 eV PhE for which the surface sensitivity is not extreme and which illustrates our discussion the best.

As seen the relative intensities of the components (G, S1 and S2) are greatly enhanced (comparing them to the spectrum of Fig. 2a) and dominate the spectrum. This becomes even more pronounced after increasing the photoelectron emission angle. (S1 + S2)/G ratio changes weakly upon sample tilting indicating that prevailing sources of these components are located in the top atomic layer. In contrast the SiC component changes considerably which means that its sources are located below the top layer. At minimum probing depth, (350 eV PhE, 65° emission angle) corresponding roughly to 1 ML of carbon, this component is hardly observable. The rest of the collected SXPS data is fully compatible with the above conclusions ensuring that we have properly interpreted this results as the emitter depth-induced effect and have not mistaken it with a photoelectron diffraction or other phenomena. The spectra don't show the presence of a SiC′ component which would be observed only if the graphitization process was reversed further, leaving the SiC surface at least partially free from the graphene and the buffer layer. These results show that the SiC re-growth happens beneath the surface, at the interface between graphene/buffer-layer and bulk SiC.

A comment is also due regarding the LEED pattern shown in Fig. 2f, observed after converting graphene back to SiC through annealing the surface for 210 min, corresponding to the SiC' phase. A number of diffraction spots, constituting the pattern is very large and they may even seem accidentally scattered. Contrary to this first impression, the surface is well ordered, having large coherent domains, which is clearly indicated by the sharp diffraction spots and low incoherent background signal, particularly at lower electron energies (not shown here). After a careful check the pattern appears perfectly p6m symmetric, therefore it is undoubtely a case of a hexagonal reconstruction. In general, case, the hexagonal, reconstruction which we may describe using Wood's notation as:

$$(\sqrt{n^2+m^2+nm} \times \sqrt{n^2+m^2+nm})R\left(ArcCos\frac{2n+m}{2\sqrt{n^2+m^2+nm}}\right) \quad (1)$$

n,m being any integer numbers ≥ 0, destroys the surface lattice mirror symmetries, however, two equivalent reconstructed domains (corresponding to interchanging n and m) rotated in the opposite directions are possible, which eventually results in the mirror symmetries observed in the diffraction pattern. Also, due to the inherent presence of left and right rotated domains, each basic (1x1) spot becomes surrounded with the ring of twelve closest diffraction spots, having the radius equal to reciprocal reconstructed lattice constant (only for the special case of 30° rotation, left and right domains are redundant and in this case the "usual" hexagonal pattern is observed). Within the ring, the spots are mirror-symmetrically arranged, with reference to the symmetry axes of the basic lattice, at angles corresponding to the reconstruction angle. Thus by examination of the neighborhood of some (1x1) spot, both the reconstruction rotation angle, and the reconstruction factor can be relatively easily identified. Such an analysis is shown in Fig. 5. We identify three families of spots denoted in Fig. 5 by differently colored circles and ticks. Not all the diffraction spots are seen due to the effect of form factors, but their number is sufficient to conclude that we have to do with three sets of spots: (4.6 × 4.6) R ± 11.5°(red), (4.6 × 4.6) R ± 24.5°(blue), (4.0 × 4.0) R ± 19.8°(green). The errors of the presented numbers may be considerable because of the distortions of the LEED imaging (due to the residual electric field and the projection) but we estimate them as not more than 0.25 for the factor, and 1° for the angle (where we expect slightly too large angles read, due to the specific distortions observed in our diffractograms). These accuracies are, nevertheless, entirely sufficient to unambiguously decode the reconstruction type. These experimental data indicate the presence of the following theoretical reconstructions: $(\sqrt{21} \times \sqrt{21})R \pm 10.89^{\circ}$ and $(\sqrt{19} \times \sqrt{19})R \pm 23.4^{\circ}$,[or: ~(4,58 × 4,58)R1 ± 0.9° and ~(4,36x4,36)R ± 23.4°]. For the 19,8°

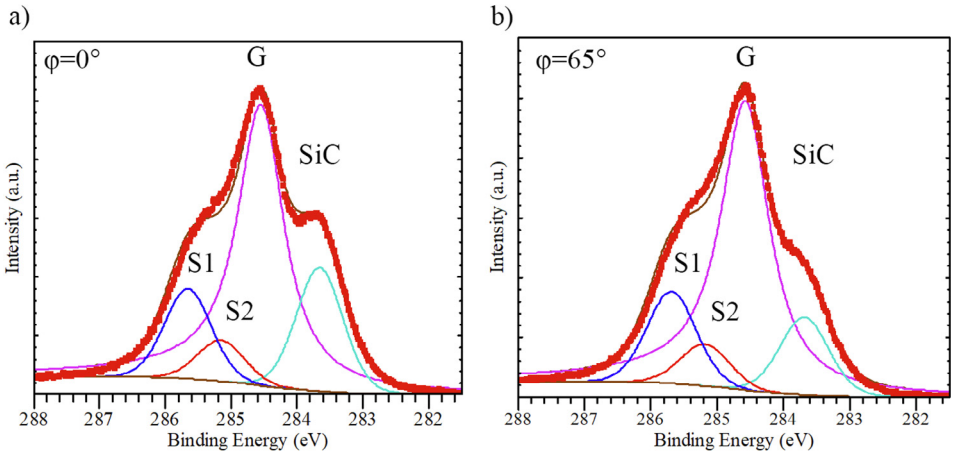

Fig. 4. XPS spectra in the C1s region, of the sample with partly reversed graphitization, measured for the photoelectron emission angle, with respect to the normal to the surface, equal to: a) 0° and b) 65°.

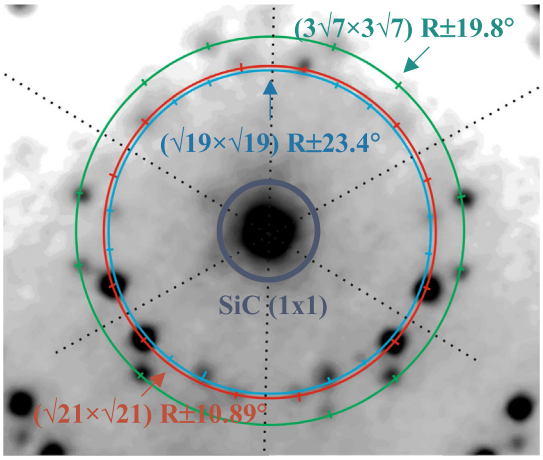

Fig. 5. Enlarged part of the low energy electron diffractogram acquired for the sample, for which the graphene film has been converted back to SiC (incident electron energy is equal to 200 eV). Mirror symmetry axes of the basic lattice are indicated by the dashed lines and the three spot families are identified by blue, red and green circles and ticks.

rotated set, no corresponding hexagonal reconstruction is found in the way described above, however, there exist a related reconstruction$(3\sqrt{7} \times 3\sqrt{7})R \pm 19.1^{\circ}$[or $(7, 93x7, 93)R \pm 19.1^{\circ}$],having the proper angle but a doubled reconstruction factor. Such a reconstruction might explain our green set of spots, if the ring of features nearest to the basic spot was erased by an action of the form factor and we were observing only the spots belonging to the second, larger ring. This larger ring should be composed of 24 diffraction spots: 12 of them distant from the basic spot by double reciprocal lattice constant and rotated by the reconstruction angle and 12 other at the $2/\sqrt{3}$ shorter distance and rotated further by 30°. In our case we see the 12 "doubled" spots indicated as the green set. The other 12 spots happen to coincide with the spots of the red set. Concluding, the surface under discussion is covered with $(3\sqrt{7} \times 3\sqrt{7})R \pm 19.1^{\circ}$ and $(\sqrt{19} \times \sqrt{19})R \pm 23.4^{\circ}$reconstructed domains and the $(\sqrt{21} \times \sqrt{21})R \pm 10.89^{\circ}$ domains cannot be excluded without additional analysis.

Although not exactly the same the observed surface phase bears similarity to the Si-rich phases on 6H-SiC(0001) surface reported by Starke et al. [21] and Heinz et al. [22]. Those phases have their Si content between that of 3 × 3 and $(\sqrt{3} \times \sqrt{3})$ SiC phases. The particular sample discussed here has been taken out to air with reference to AFM studies, however, many other samples have been graphitized in a similar way, converted back to SiC and recycled to 3 × 3 reconstruction for further studies.

Similar studies regarding graphitization blocking by an external Si flux, albeit without graphitization reversal phase, were performed by F.J. Ferrer, et. al. [23]. In their study, 4H SiC (0001) samples were annealed at the temperatures of up to 1100 °C and Si flux of up to 2.0×10^{13} cm^{-2} s^{-1}, resulting in an atomically flat step-terrace structure of the final surface. Both the initial (before annealing in the Si flux) and the final surface phase, obtained in the study, was a (√3×√3) R30° reconstruction; the authors didn't detect (3 × 3) or (6√3 × 6√3) R30° reconstructions in their experimental conditions. This makes it different from our study, where both the initial and the final surface phase is Si-rich (3 × 3) reconstruction. The structure of the two phases is similar and consists of Si adatoms bound to sub-surface Si atoms, located in either bulk SiC, in case of (√3×√3)R30° reconstruction, or in an additional Si adlayer positioned on top of bulk SiC, in case of (3 × 3) reconstruction [20,24]. The key difference between the two is an additional Si adlayer, separating topmost Si adatoms from bulk SiC. (3 × 3) reconstruction is usually formed in Si-rich conditions, in temperatures around 100 °C lower than the (√3 × √3)R30° reconstruction. This indicates, that the Si flux used in our work, which is an order of magnitude higher than the flux used in Ref. 22, is sufficiently high to significantly affect the stoichiometry of the initial and final surfaces and induce their enrichment in silicon. The additional Si adlayer, present in the (3 × 3) reconstruction, could have significant influence on the graphene growth in higher temperatures, in terms of inhibiting step flow and decreasing the erosion rate of the terrace edges.

It is clear that the growth of epitaxial graphene on silicon carbide may benefit from using the highest attainable process temperature since this would increase the mobility of carbon atoms on the surface and improve the homogeneity and quality of graphene films. The same ordering effects could be in principle obtained with longer process times. However, when aiming at high-quality few-layer graphene films, the possible process temperatures/times are limited by the sublimation rate of Si from SiC surface and they are far from being adequate. In case of Si beam-assisted graphitization, the additional factor helping to independently regulate the process temperature and time is the Si flux density. In our experimental setup, the maximum achievable flux is 2.5×10^{14} cm^{-2} s^{-1}. This is sufficiently high to inhibit SiC (0001) graphitization up to the temperature of 1350 °C. As shown before, the graphitization can be also reversed in this Si flux at the slightly lowered process temperature.

Having this, we investigate a new process flow, enabling a synthesis of the few-layers graphene. Within our slow scheme (Fig. 1) and with a constant Si flux of 2.5×10^{14} cm^{-2} s^{-1}, the surface is annealed to increasingly higher temperatures. Graphene film crystallizes when the sample is at the temperatures for which the reaction equilibrium shifts towards the product side and then reduction of its thickness occurs when the sample is slowly cooled down and the reaction equilibrium shifts towards the substrate side. Using this process, we are able to anneal SiC (0001) at the temperatures up to 1495 °C, without forming any graphene after cooldown. As a reference, the samples treated using the fast scheme, with the same maximal temperature and the same Si flux, are characterized by the graphene coverage of 1.5ML, which is setting the lower limit for the maximal graphene coverage during the slow process. We may compare the maximal graphene coverages for the two schemes directly, since during the slow process, any excess Si possibly present at the beginning of the process must be lost from the surface well below the temperature at which the graphene formation begins [25]. The complete reduction of 1.5 ML graphene also means the restoration of at least 6 SiC bilayers (on average, growth of a monolayer graphene requires decomposition of 3 SiC bilayers [26]). We have found that, the annealing temperatures, which result in a detectable graphene coverage are 1350 °C and 1500 °C correspondingly within the fast and the slow process scheme. It is likely that using even lower rates (which would be impractical), or higher Si flux (which could easily be obtained, for example from e-beam type source) would allow for further increase of the process temperature even to values exceeding temperatures commonly used in the atmospheric-pressure graphitization (which can be as high as 2000 °C [27]).

In Fig. 6a C1s XPS peak for the sample annealed at T = 1500 °C is shown. The peak consists of 5 main components: G (assigned to graphene), SiC (assigned to silicon carbide beneath graphene and buffer layer), S1, S2 (assigned to buffer layer) and SiC' (assigned to the surface of SiC restored during the cooldown (Si + G)), which were previously described. The relative intensity of the SiC' component is equal to around 30%, which can be associated with the fraction of the surface with restored SiC.

AFM maps – see Fig. 6b – show that, as already suggested by the XPS results, the surface of the sample is inhomogeneous. The presence of islands on terraces, elongated usually alongside the terrace edge is observed, with the height between 0.75 and 1.5 nm, relative to the underlying terrace - see the line profile in Fig. 6c taken along the line marked in Fig. 6b. Three SiC bilayers with the height of 0.75 nm are consumed for the creation of a single graphene layer, so it is likely that the 0.75 nm islands are the result of the "consumption" of a single graphene layer, while the 1.5 nm islands are a result of the

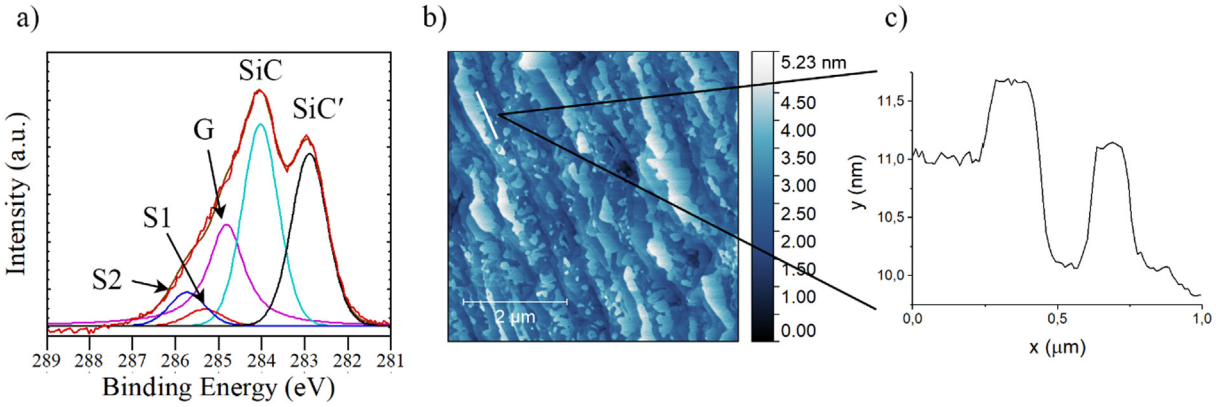

Fig. 6. a) XPS spectrum, b) AFM scan and c) line profile, taken along the line shown in Fig. 6b, of a SiC sample processed at T = 1500 °C, using the slow scheme.

"consumption" of both graphene and buffer layer, occurring during the reversal of the graphitization process.

Utilizing the slow process scheme we have also grown samples of: bilayer graphene, with the maximum process temperature of T = 1700 °C, tetralayer graphene, with T = 1750 °C and 5-layer graphene with T = 1810 °C. ARPES spectra of the samples are shown in Fig. 7:

Number of graphene layers is determined by counting the number of electron bands visible in the ARPES spectra. In case of bi-/tetra-layer graphene, 2/4 bands are clearly visible, while in case of 5-layer material, the fifth band is somewhat less pronounced (it is marked by a dashed arrow in Fig. 7d). Synthesized graphene is, in all cases, n-doped, consistently with the expected influence of the underlying buffer layer [28]. In case of tetralayer graphene, the band structure is characteristic for the predicted structure of ABC-stacked graphene [29]. This is consistent with observations of other groups, who found that ABC-stacked graphene forms preferentially on SiC (0001) [30], although the growth of up to three layers of graphene has been demonstrated [31].

All obtained dispersion map contain characteristic flat parts of the electron band(s) located near the Fermi energy (marked by white, solid arrows in Fig. 7), which are often referred to as "Sombrero" structures. The presence of flat bands means also that high density of states exists in a narrow energy range. This has been studied before for bilayer graphene and identified as 2D-extended van Hove singularity [32]. Due to the indications of enhanced electron–phonon coupling, it was theorized that this could help achieving superconductivity of graphene. Spectrum of tetra-layer graphene confirms the presence of two flat parts of the electron bands, while the electronic structure of 5-layer graphene contains an additional, third flat part, near the Fermi level, as shown in detail in Fig. 8

Detailed spectra taken near Fermi energy, shown in Fig. 8, reveal, that in case of tetra- and 5-layer graphene, the upper bands (located at $E_B \approx 0.15$ eV) might show some dispersion near the K point of the reciprocal lattice, creating a small, but detectable "kink". Additional flat band in 5-layer graphene is located at $E_B = 0.07$ eV. To our knowledge, it is one of the first observations of multiple flat bands in a few-layers graphene grown on 4H-SiC (0001), since most literature examples of flat bands focus on rhombohedral graphene grown on 3C-SiC (1 1 1) [33,34].

We have used AFM to investigate surface morphology of the obtained samples. AFM maps of bi-, and tetra-layer graphene (Fig. 9a, b, respectively), show that the surfaces are well ordered and homogeneously covered in steps of average width of around 0.25–0.5 μm, as shown in the exemplary profile in Fig. 9d. The surface of a 5-layer graphene (Fig. 9c) is more rough, containing pits, with the depth of 10–20 nm. Its step structure is scarcely visible likely because of AFM

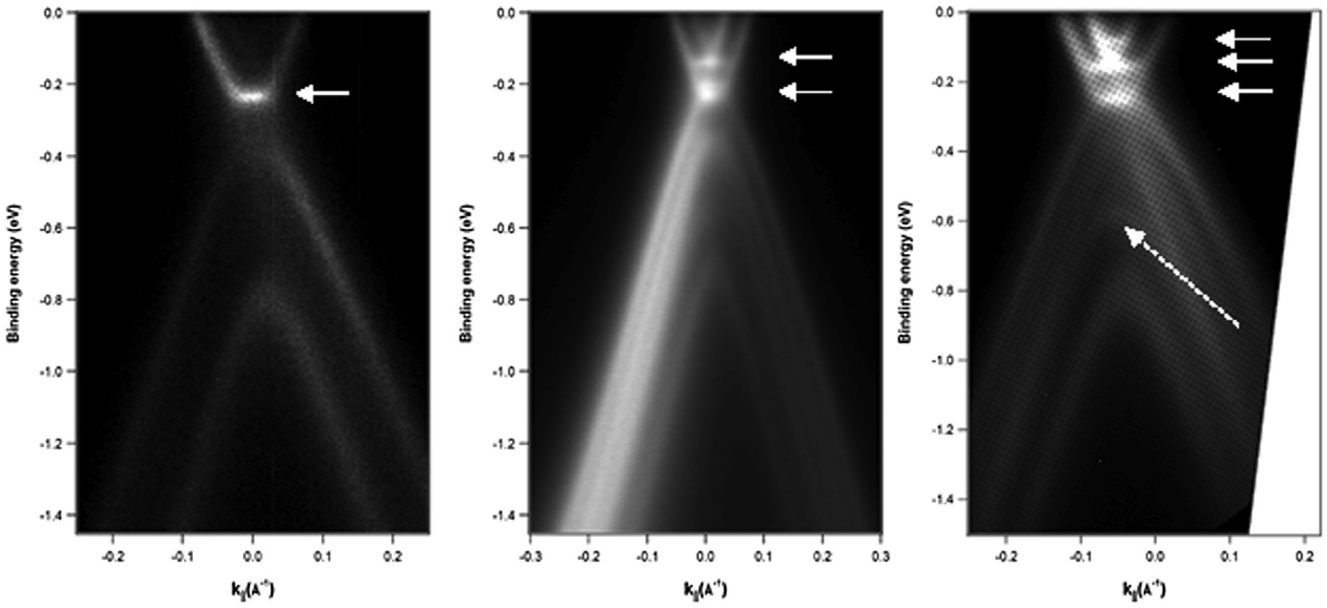

Fig. 7. ARPES spectra around the K point of the reciprocal lattice of: a) bi-, b) tetra- and c) 5-layer graphene grown using the slow scheme at: a) T = 1700 °C; b) T = 1750 °C; and c) T = 1810 °C (wavevector relative to the K point).

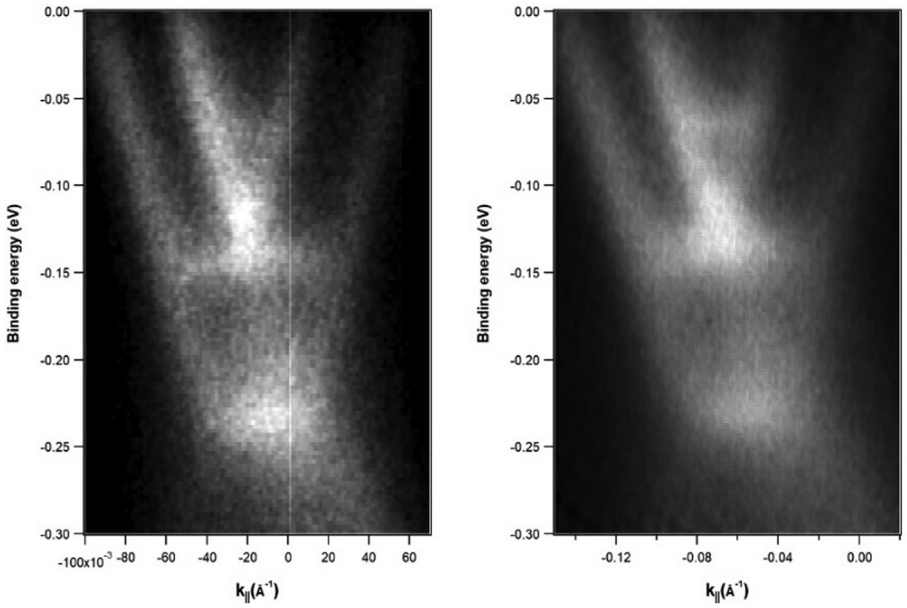

Fig. 8. ARPES spectra around the K point of the reciprocal lattice of: a) tetra- b) 5-layer graphene.

artefacts. The presence of such pits indicates that in temperatures above 1810 °C higher Si flux is needed to control the graphitization process. Formation of deep pits during graphene formation has been reported, although their depth was usually smaller then in our case and equal to around 6 nm [35].

The steps found on the surface covered with bilayer graphene have the height between 0.25 and 2.5 nm, i.e., between 1 and 10 SiC bilayers (with the average of 0.7 nm, close to 3 SiC bilayers), while the steps found on the surface covered with tetralayer graphene have the height between 0.25 and 2.75 nm, i.e., between 1 and 11 SiC bilayers (with the average of 1.1 nm, close to 4 SiC bilayers). Similar values are found for all samples prepared using our slow scheme, which is somewhat surprising, since other growth methods developed for G/SiC(0001) often result in the formation of macro-steps on the surface having heights of several tens of nanometers [5]. Macro-steps present at the surfaces of epitaxial graphene on SiC are considered to be a major issue, hindering its applications in useful devices. Substantial effort has been put in recent years into understanding step-bunching phenomena occurring during graphene growth and minimizing its effects. Bao J. et al. has reported step heights of 0.75–1.5 nm, using sequential control of step bunching [15], while Kruskopf M., et. al. reported step heights between 0.25 and 2.5 nm [16], utilizing polymer adsorbate for the enhanced buffer layer nucleation. We note here, that the method of partially reversible graphitization in Si flux is comparable to the best literature examples, even though its optimization potential is far from being exhausted.

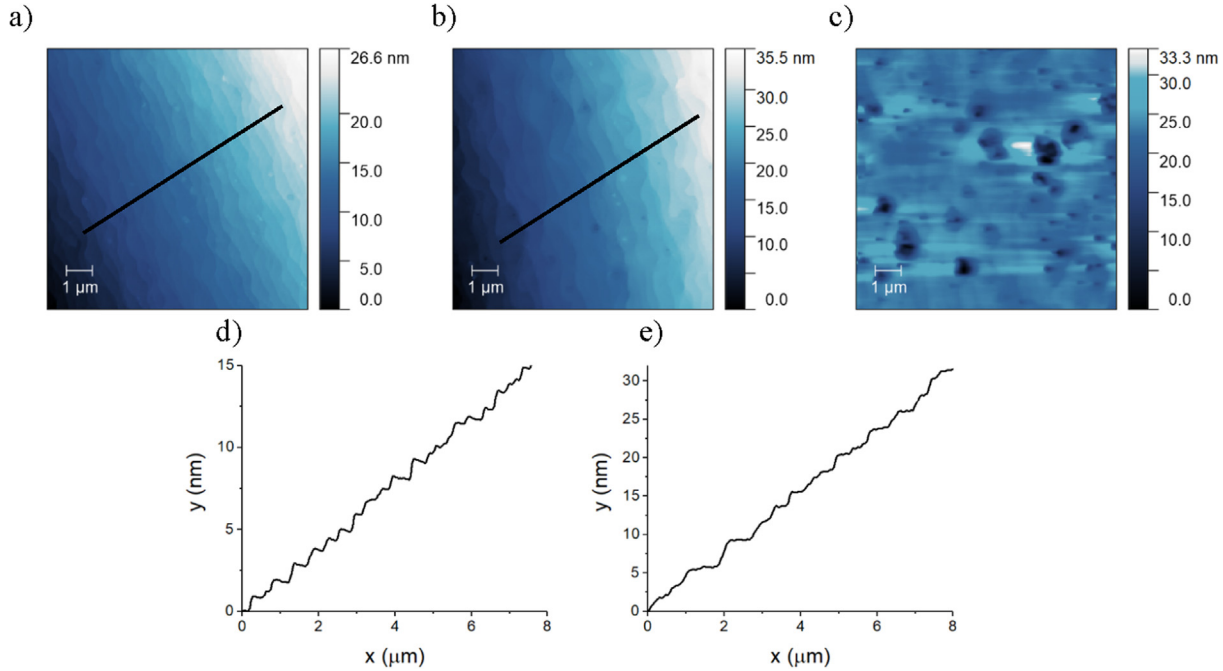

Fig. 9. AFM images of a: a) bi-, b) tetra- and c) 5-layer graphene (the same samples as in Fig. 7) grown using the slow scheme at: a) T = 1700 °C; b) T = 1750 °C; and d) T = 1810 °C; d) line profile, taken along the line shown in Fig. 9a; e) line profile, taken along the line shown in Fig. 9b.

Amount of the step-bunching on the G/SiC(0001) surface has been previously linked to the heating rate of the substrate, however, previous reports seem to be contradictory to our findings. While in our case, low heating and cooling rate resulted in the minimal step-bunching on the surface, Bao J., et al., have found, during their experiments concerning graphene growth in atmospheric pressure buffer gas [15] that the low heating rate increases step-bunching. They found also that the step bunching occurs to the highest extent at the temperatures between 1200 ˚C and 1600 ˚C, below the temperature of graphene formation, while the graphene film on the surface actually inhibits the step bunching. Long annealing below graphene formation temperature inevitably leads to the formation of macro-steps at the surface.

The key difference between the method studied here and the atmospheric-pressure buffer assisted graphitization [5], is that external Si atomic beam may shift the surface stoichiometry to the Si-rich while at the absence of such beam it tends to be Si deficient. This should not be understood as a formation of solid Si on surface. Fissel et al. [36] reported that SiC(0001) 3×3 surface does not accumulate excess Si even at temperatures as low as 900 ˚C. Nevertheless, the Si atoms coming on the surface with the considerable rate of 2.5×10^{14} cm^{-2} s^{-1}, (corresponding to growth rate of 30 Å/min, if 100% condensation occurred) have certain residence time on the surface and at step edges. Results obtained here show that their transient presence is sufficient to inhibit graphitization up to the temperatures 1350 ˚C and on the other hand it strongly reduces the surface step flow/bunching.

4. Conclusions

We have demonstrated the reversibility of the thermal decomposition of SiC (0001) surface in the Si-rich environment. On this basis, we have developed a new approach to the synthesis of high-quality, few-layer graphene on the minimally step bunched SiC (0001) surface, through very slow heating and cooling of SiC under the flux of Si atoms. The optimization potential of the approach is far from exhausted, but it already seems promising for future applications, as it yields high-quality material, directly on an insulating substrate, in a simple, single-step, UHV-compatible process. It also allows for increasing process time and temperature, without inducing step-bunching on the surface. Multilayer graphene formed in this process is characterized by the appearance of multiple flat-bands in the ARPES spectra, which can be particularly interesting for the future studies of its superconductivity. We expect that this method will be relevant for the development of future commercial, wafer-scale epitaxial graphene technologies. These results are also relevant for other growth techniques, as they show that controlling heating and cooling rates is important for process design and optimization.

CRediT authorship contribution statement

Piotr Ciochoń: Conceptualization, Methodology, Formal analysis, Investigation, Data curation, Writing - original draft, Writing - review & editing, Visualization, Project administration, Funding acquisition. **Mateusz Marzec:** Investigation, Resources, Data curation. **Natalia Olszowska:** Formal analysis, Investigation, Resources, Data curation. **Jacek Kołodziej:** Conceptualization, Methodology, Formal analysis, Investigation, Resources, Data curation, Writing - review & editing, Supervision, Funding acquisition.

Declaration of Competing Interest

The authors declare that they have no known competing financial interests or personal relationships that could have appeared to influence the work reported in this paper.

Acknowledgements

We would like to express our gratitude for Bartosz Such for his help with the AFM measurements. Part of the experiments was performed at the SOLARIS National Synchrotron Radiation Centre, at the ARPES beamline. The experiments were performed thanks to the collaboration of the SOLARIS Staff. We would like to acknowledge the financial support of National Science Centre, Poland (grant no. 2014/15/N/ST5/00523) and Polish Ministry of Science and Higher Education (decision no. 7150/E-338/M/2015). The research was partly supported by the Polish Ministry of Science and Higher Education within the framework of Inkubator Innowacyjności + programme (decision no. 14.2017 2017-06-29)

References

[1] Y.M. Lin, A. Valdes-Garcia, S.J. Han, D.B. Farmer, I. Meric, Y. Sun, Y. Wu, C. Dimitrakopoulos, A. Grill, P. Avouris, K.A. Jenkins, Wafer-scale graphene integrated circuit, Science (80-) 332 (2011) 1294–1297, https://doi.org/10.1126/science.1204428.

[2] T. Yager, A. Lartsev, R. Yakimova, S. Lara-Avila, S. Kubatkin, Wafer-scale homogeneity of transport properties in epitaxial graphene on SiC, Carbon N. Y. 87 (2015) 409–414, https://doi.org/10.1016/j.carbon.2015.02.058.

[3] S. Hertel, D. Waldmann, J. Jobst, A. Albert, M. Albrecht, S. Reshanov, A. Schöner, M. Krieger, H.B. Weber, for monolithic wafer-scale electronics, Nat. Commun. 3 (2012) 957, https://doi.org/10.1038/ncomms1955.

[4] D.V. Badami, Graphitization of α-silicon carbide, Nature 193 (1962) 569.

[5] K.V. Emtsev, A. Bostwick, K. Horn, J. Jobst, G.L. Kellogg, L. Ley, J.L. Mcchesney, T. Ohta, S.A. Reshanov, J. Röhrl, E. Rotenberg, A.K. Schmid, D. Waldmann, H.B. Weber, T. Seyller, Towards wafer-size graphene layers by atmospheric pressure graphitization of silicon carbide, Nat. Mater. 8 (2009) 203–207, https://doi.org/10.1038/nmat2382.

[6] W.A. De Heer, C. Berger, M. Ruan, M. Sprinkle, X. Li, Y. Hu, B. Zhang, J. Hankinson, E. Conrad, Large area and structured epitaxial graphene produced by confinement controlled sublimation of silicon carbide, Proc. Natl. Acad. Sci. U. S. A. 108 (2011) 16900–16905, https://doi.org/10.1073/pnas.1105113108.

[7] G. Deokar, J. Avila, I. Razado-Colambo, J.L. Codron, C. Boyaval, E. Galopin, M.C. Asensio, D. Vignaud, Towards high quality CVD graphene growth and transfer, Carbon 89 (2015) 82–92, https://doi.org/10.1016/j.carbon.2015.03.017.

[8] H. Wang, G. Yu, Direct CVD graphene growth on semiconductors and dielectrics for transfer-free device fabrication, Adv. Mater. 28 (2016) 4956–4975, https://doi.org/10.1002/adma.201505123.

[9] L. Banszerus, M. Schmitz, S. Engels, M. Goldsche, K. Watanabe, T. Taniguchi, B. Beschoten, C. Stampfer, Ballistic transport exceeding 28 μm in CVD grown graphene, Nano Lett. 16 (2016) 1387–1391, https://doi.org/10.1021/acs.nanolett.5b04840.

[10] G.G. Jernigan, B.L. VanMil, J.L. Tedesco, J.G. Tischler, E.R. Glaser, A. Davidson, P.M. Campbell, D.K. Gaskill, Comparison of epitaxial graphene on si-face and C-face 4H SiC formed by ultrahigh vacuum and RF furnace production, Nano Lett. 9 (2009) 2605–2609, https://doi.org/10.1021/nl900803z.

[11] Y. Liu, L. Chen, D. Hilliard, Q.S. Huang, F. Liu, M. Wang, R. Böttger, R. Hübner, A.T. N'Diaye, E. Arenholz, V. Heera, W. Skorupa, S. Zhou, Controllable growth of vertically aligned graphene on C-face SiC, Sci. Rep. 6 (2016) 1–10, https://doi.org/10.1038/srep34814.

[12] S. Tanaka, K. Morita, H. Hibino, Anisotropic layer-by-layer growth of graphene on vicinal SiC (0001) surfaces, Phys. Rev. B 81 (2010) 041406, , https://doi.org/10.1103/PhysRevB.81.041406.

[13] M. Sprinkle, M. Ruan, Y. Hu, J. Hankinson, B. Zhang, X. Wu, C. Berger, W.A. De Heer, Scalable templated growth of graphene nanoribbons on SiC, Nat. Nanotechnol. 5 (2010) 727–731, https://doi.org/10.1038/nnano.2010.192.

[14] M. Ridene, T. Wassmann, E. Pallecchi, G. Rodary, J.C. Girard, A. Ouerghi, Epitaxial graphene on step bunching of a 6H-SiC(0001) substrate: aromatic ring pattern and Van Hove singularities, Appl. Phys. Lett. 102 (2013), https://doi.org/10.1063/1.4796170.

[15] J. Bao, O. Yasui, W. Norimatsu, K. Matsuda, M. Kusunoki, Sequential control of step-bunching during graphene growth on SiC (0001), Appl. Phys. Lett. 109 (2016), https://doi.org/10.1063/1.4961630.

[16] M. Kruskopf, D.M. Pakdehi, K. Pierz, S. Wundrack, R. Stosch, T. Dziomba, M. Götz, J. Baringhaus, J. Aprojanz, C. Tegenkamp, J. Lidzba, T. Seyller, F. Hohls, F.J. Ahlers, H.W. Schumacher, Comeback of epitaxial graphene for electronics: Large-area growth of bilayer-free graphene on SiC, 2D Mater. 3 (2016), https://doi.org/10.1088/2053-1583/3/4/041002.

[17] U. Starke, C. Riedl, Epitaxial graphene on SiC(0001) and (000–1): from surface reconstructions to carbon electronics, J. Phys.: Condens. Matter 21 (2009), https://doi.org/10.1088/0953-8984/21/13/134016.

[18] P. Ciochoń, Ł. Bodek, M. Garb, Ł. Zając, J.J. Kołodziej, Si beam-assisted graphitization of SiC (0001), Appl. Phys. A Mater. Sci. Process. 124 (2018) 1–9, https://doi.org/10.1007/s00339-018-2145-9.

[19] C. Xia, S. Watcharinyanon, A.A. Zakharov, R. Yakimova, L. Hultman, L.I. Johansson, C. Virojanadara, Si intercalation/deintercalation of graphene on 6H-SiC(0001), Phys. Rev. B – Condens. Matter Mater. Phys. 85 (2012) 1–7, https://doi.

org/10.1103/PhysRevB.85.045418.
[20] A. Jablonski, Practical expressions for the mean escape depth, the information depth, and the effective attenuation length in Auger-electron spectroscopy and x-ray photoelectron spectroscopy, J. Vac. Sci. Technol., A 27 (2009) 253, https://doi.org/10.1116/1.3071947.
[21] U. Starke, J. Schardt, J. Bernhardt, M. Franke, K. Heinz, Stacking transformation from hexagonal to cubic SiC induced by surface reconstruction: a seed for heterostructure growth, Phys. Rev. Lett. 82 (1999) 2107–2110.
[22] K. Heinz, L. Hammer, J. Hass, W.A. De Heer, E.H. Conrad, Functional surface reconstructions of hexagonal SiC, J. Phys.: Condens. Matter 16 (2004) S1705–S1720, https://doi.org/10.1088/0953-8984/16/17/013.
[23] F.J. Ferrer, E. Moreau, D. Vignaud, S. Godey, X. Wallart, Semicond. Sci. Technol. 24 (2009) 125014, , https://doi.org/10.1088/0268-1242/24/12/125014.
[24] J. Schardt, J. Bernhardt, U. Starke, K. Heinz, Crystallography of the (3×3) surface reconstruction of $3C-SiC(111)$, $4H-SiC(0001)$, and $6H-SiC(0001)$ surfaces retrieved by low-energy electron diffraction, Phys. Rev. B – Condens. Matter Mater. Phys. 62 (2000) 10335, https://doi.org/10.1103/PhysRevB.62.10335.
[25] T. Tomooka, Y. Shoji, T. Matsui, High temperature vapor pressure of Si, J. Mass Spectrom. Soc. Jpn. 47 (1999) 49–53, https://doi.org/10.5702/massspec.47.49.
[26] J. Hass, W.A. De Heer, E.H. Conrad, The growth and morphology of epitaxial multilayer graphene, J. Phys.: Condens. Matter 20 (2008), https://doi.org/10.1088/0953-8984/20/32/323202.
[27] C. Bouhafs, V. Darakchieva, I.L. Persson, A. Tiberj, P.O.Å. Persson, M. Paillet, A.A. Zahab, P. Landois, S. Juillaguet, S. Schöche, M. Schubert, R. Yakimova, Structural properties and dielectric function of graphene grown by high-temperature sublimation on 4H-SiC(000–1), J. Appl. Phys. 117 (2015), https://doi.org/10.1063/1.4908216.
[28] J. Ristein, S. Mammadov, T. Seyller, Origin of doping in quasi-free-standing graphene on silicon carbide, Phys. Rev. Lett. 108 (2012) 1–5, https://doi.org/10.1103/PhysRevLett.108.246104.
[29] H. Min, A.H. MacDonald, Electronic structure of multilayer graphene, Prog. Theor. Phys. Suppl. (2008) 227–252, https://doi.org/10.1143/PTPS.176.227.
[30] W. Norimatsu, M. Kusunoki, Selective formation of ABC-stacked graphene layers on SiC(0001), Phys. Rev. B – Condens. Matter Mater. Phys. 81 (2010) 1–4, https://doi.org/10.1103/PhysRevB.81.161410.
[31] K. Sugawara, N. Yamamura, K. Matsuda, W. Norimatsu, M. Kusunoki, T. Sato, T. Takahashi, Selective fabrication of free-standing ABA and ABC trilayer graphene with/without Dirac-cone energy bands, NPG Asia Mater. 10 (2018) e466, , https://doi.org/10.1038/am.2017.238.
[32] D. Marchenko, D.V. Evtushinsky, E. Golias, A. Varykhalov, T. Seyller, O. Rader, Extremely flat band in bilayer graphene, Sci. Adv. 4 (2018) 1–8, https://doi.org/10.1126/sciadv.aau0059.
[33] W. Wang, Y. Shi, A.A. Zakharov, M. Syväjärvi, R. Yakimova, R.I.G. Uhrberg, J. Sun, Flat-band electronic structure and interlayer spacing influence in rhombohedral four-layer graphene, Nano Lett. 18 (2018) 5862–5866, https://doi.org/10.1021/acs.nanolett.8b02530.
[34] D. Pierucci, H. Sediri, M. Hajlaoui, J. Girard, T. Brumme, M. Calandra, E. Velez-fort, G. Patriarche, M.G. Silly, G. Ferro, G. Yvette, I. De Minéralogie, D.P. Matériaux, D. Cosmochimie, U.M.R. Cnrs, S. Universités, Evidence for flat bands near the fermi level in epitaxial rhombohedral multilayer graphene, ACS Nano 9 (2015) 5432–5439, https://doi.org/10.1021/acsnano.5b01239.
[35] J.B. Hannon, R.M. Tromp, Pit formation during graphene synthesis on SiC(0001): in situ electron microscopy, Phys. Rev. B – Condens. Matter Mater. Phys. 77 (2008) 1–4, https://doi.org/10.1103/PhysRevB.77.241404.
[36] A. Fissel, K. Pfennighaus, U. Kaiser, B. Schröter, Mechanisms of homo- and heteroepitaxial growth of SiC on α -SiC (0001) by solid-source molecular beam epitaxy, J. Electron. Mater. 28 (1999) 206–213.